Nonstatistical γ emission in ^{3}He- and α-induced reactions

J. A. Behr,* K. A. Snover, C. A. Gossett, G. Feldman, J. H. Gundlach, and M. Kicińska-Habior†
Nuclear Physics Laboratory, University of Washington, Seattle, Washington 98195
(Received 21 September 1995)

We have measured inclusive γ-ray production cross sections for ^{3}He- and α-induced reactions on various targets in the mass range $A=61-181$ at projectile energies of 11–27 MeV. Except for α-induced yields on the lightest targets, all reactions show high-energy γ-ray yields 1–3 orders of magnitude larger than can be obtained from statistical model calculations. Angular distributions are strongly forward peaked in the center of mass frame for the highest γ-ray energies, providing model-independent evidence for a nonstatistical reaction mechanism. Calculations of direct radiative capture and semidirect excitation of the giant dipole resonance can qualitatively reproduce the angular distributions but cannot reproduce either the dependence of the γ-ray cross sections on E_γ or the target dependence of the absolute cross sections. The ^{12}C(^{3}He,γ_0)^{15}O reaction was found to change from predominantly statistical to predominantly direct over this bombarding energy range.

PACS number(s): 25.55.−e, 24.60.Dr, 24.30.Cz, 23.20.−g

I. INTRODUCTION

The reaction mechanisms for radiative capture of nucleons and heavy ions in certain energy regimes are reasonably well established. The radiative capture of energetic nucleons up to nucleon energies of at least 25 MeV is dominated by the direct and semidirect processes. In direct radiative capture, the nucleon is captured directly into a final state, radiating in the process. In semidirect radiative capture, the reaction proceeds primarily through single-step excitation of the giant dipole resonance (GDR), which then radiates.

In contrast, heavy ion radiative capture up to projectile energies of at least 5 MeV/A in medium and heavy nuclei is well described by fusion leading to a statistically equilibrated compound nucleus, which then decays with a strength function dominated by the GDR [1]. At higher heavy ion projectile energies, $E_{\rm proj} \gtrsim 20$ MeV/A, γ rays with energy 100 MeV and higher have been observed [2]. In this energy regime there is experimental and theoretical support for a reaction mechanism involving bremsstrahlung from incoherent neutron-proton collisions between projectile and target nucleons. Coherent collective nuclear bremsstrahlung, in which the projectile is accelerated by the mean field of the target and radiates in the process, has also been proposed as a possible reaction mechanism [3]; however, there exists no clear evidence for this process.

In the course of studying statistical GDR decay in complex particle collisions, we first noted anomalously large yields of high-energy γ rays from ^{3}He and α collisions with Sm target nuclei [1]. In this work, we present an exploration of the systematics of this effect by measurements of inclusive γ-ray production cross sections from ^{3}He- and α-induced reactions on various targets in the mass range $A=61-181$ at projectile energies of 11–27 MeV. These projectile masses and energies fall between the extremes of nucleon-induced γ-ray production and statistical heavy-ion-induced reactions, and thus one might expect features of both direct-semidirect (DSD) and statistical radiative capture.

Our measured γ-ray spectra from the ^{3}He- and α-induced reactions share a number of common features. In all the reactions, large structureless γ yields are observed in and above the giant dipole resonance region ($E_\gamma \geqslant 14$ MeV). Except for α-induced reactions on the lightest targets, all reactions show high-energy γ-ray yields which are 1–3 orders of magnitude larger than statistical model calculations of compound nuclear decay.

Angular distributions have been measured for several cases; they are strongly forward peaked in the center of mass frame for the highest γ-ray energies, providing model-independent evidence for a nonstatistical reaction mechanism. The forward-peaked angular distributions also imply the presence of interfering multipoles of opposite parity, most likely $E1$ and $E2$. The degree of forward peaking in the c.m. frame cannot be described in terms of emission from a moving source with a single source velocity, as has been found for heavy ion collisions at higher bombarding energy.

For reactions initiated by both projectiles, γ rays are observed that carry close to the total energy available in the reaction, suggesting a coherent production mechanism. We have also found that there is a systematic dependence of the exponential slopes and magnitudes of the high-E_γ spectra on the total energy available in the reaction.

The observed nonstatistical γ yields are in general greater for the ^{3}He projectile than for the α. This is what one would expect for $E1$ radiation from the DSD mechanism. Because the α+target systems have a small $E1$ effective charge q_{E1} ($q_{E1}=0$ for α plus an $N=Z$ target since the dipole moment vanishes in the center of mass) the direct $E1$ radiation is suppressed. Semidirect excitation of the GDR by the isospin $T=0$ α particle is isospin forbidden. However, at these γ-ray energies $k_\gamma R$ is large enough (~ 0.5 for $A = 150$ and $E_\gamma = 20$ MeV) for direct $E2$ radiation to be important.

In an attempt to quantify these simple considerations, we have performed distorted-wave calculations of the DSD pro-

*Present address: TRIUMF, 4004 Westbrook Mall, Vancouver, British Columbia V6T 2A3, Canada.
†Permanent address: Institute of Experimental Physics, University of Warsaw, 00681, Poland.

cess. These calculations indicate that even for the ^{3}He projectile the semidirect contribution is small compared to the direct contribution. The angular distributions are qualitatively reproduced by interference of direct $E1$ and $E2$ radiation. Although the yield of the highest-energy γ rays is also qualitatively reproduced, the predicted dependence on E_γ is wrong; the calculated spectrum is too flat with energy compared to the data. We conclude that direct radiative capture can account for the γ-ray yield at the highest E_γ, while some more complicated preequilibrium process must be contributing to the yield above the GDR energy.

In Sec. II below we describe the experimental technique. We present the experimental results and a phenomenological discussion in Sec. III, and we present our model calculations in Sec. IV. Several authors have performed calculations to compare with our α + ^{154}Sm and ^{3}He + ^{148}Sm data which appeared in Ref. [1]. We discuss these results together with other measurements and calculations in Sec. IV. The conclusion is Sec. V.

II. EXPERIMENT

We used ^{3}He and α beams with energy 11–28 MeV from the FN Tandem Van de Graaff at the University of Washington Nuclear Physics Laboratory. Inclusive γ-ray spectra were measured with a 10×10 in.^{2} cylindrical NaI crystal surrounded by an NE 110 plastic anticoincidence shield and by passive ^{6}LiH and paraffin neutron shielding, with 4-in.-thick Pb collimation. We bunched the beam with a pretandem bunching system and used time of flight [typical full width at half maximum (FWHM) 4 nsec, flight path of 74 cm] to distinguish between γ rays from the target and other background such as neutron-induced events from the target, eliminating the latter. Other potential sources of background such as the shielded beam dump, empty target frame, and beam collimation system were measured and found to be negligible. The anticoincidence shield, along with the time cycle of the beam, made background events from cosmic rays negligible for the γ-ray energies of interest.

Before each run the detector was calibrated up to E_γ = 22.6 MeV with discrete lines from the ^{11}B(p,γ) reaction. The detector energy resolution was $\approx$ 3.2% in the geometry used. The NaI gain was stabilized by a light-emitting diode (LED) feedback system to within 0.5%.

The absolute efficiency of the detector is experimentally known to $\pm$ 5% for γ-ray energies from 2.3 to 15.1 MeV. For $E_\gamma > 15.1$ MeV, the efficiency is determined by measuring the ratio of events rejected to events accepted by the anticoincidence shield for discrete γ rays from (p,γ_0) reactions, and assuming a total (accept + reject) efficiency that is constant above 15.1 MeV, consistent with Monte Carlo calculations. For example, this results in a relative efficiency ϵ(30 MeV)/ϵ(15 MeV) = 0.63.

Targets were self-supported rolled foils of the following thicknesses: 1.00 mg/cm^2 ^{61}Ni, 3.5 mg/cm^2 ^{62}Ni, 2.09 mg/cm^2 ^{95}Mo, 1.03 mg/cm^2 ^{96}Mo, 2.1 mg/cm^2 ^{119}Sn, 1.36 mg/cm^2 ^{120}Sn, 2.0 mg/cm^2 ^{124}Sn, 2.5 mg/cm^2 ^{148}Sm, 2.8 mg/cm^2 ^{154}Sm, and 2.0 mg/cm^2 ^{181}Ta. Target thicknesses are known to 10% from rolled material estimates, verified in many cases by energy loss of α particles from a ^{241}Am source. All targets were isotopically enriched to at least 90% except for ^{119}Sn, which was enriched to 86%.

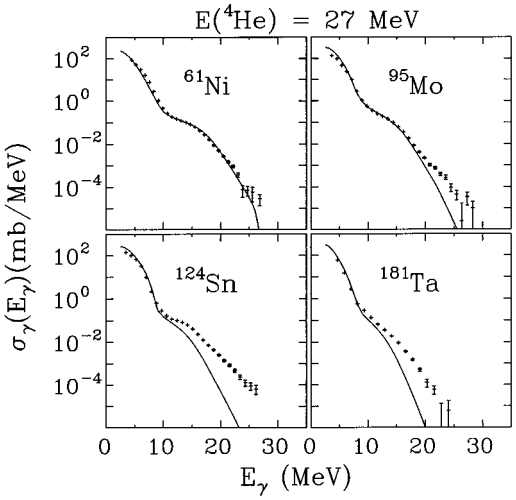

FIG. 1. Inclusive γ-ray production cross sections deduced from γ-ray spectra measured at $\theta_\gamma = 90°$, and CASCADE statistical model calculations for α+ ^{61}Ni, ^{95}Mo, ^{124}Sn, and ^{181}Ta at E(α)=27 MeV. The cross-section data shown here and in other figures do not include the efficiency correction factor discussed in Sec. III A.

Carbon and oxygen impurities in the targets were deduced from the presence of their characteristic low-energy γ rays in the spectra; spectra were measured from natural carbon and Ta_2O_5 targets and used to make corrections for impurity contributions. The largest correction for impurities was for the Sm targets; for α+ ^{148}Sm, 2% corrections were made for 15 MeV$\leq E_\gamma \leq$20 MeV, and 10% corrections for $E_\gamma >$ 20MeV; for ^{3}He+ ^{148}Sm, corrections were 15% above E_γ = 20 MeV. For all other targets the corrections were 1% or less for γ-ray energies at or above the giant dipole resonance energy.

Possible spectrum distortion from summing was found to be negligible by measuring spectra at different detector-to-target distances. This is consistent with the small absolute detector efficiency, which was 9.5 msr at E_γ = 15.1 MeV, or roughly 0.1% of 4π. Pileup was routed on line with a fast discriminator circuit found to be 50% efficient and, in addition, an off-line subtraction was made; the largest correction resulting for high-energy γ rays of interest was 7% for the 27 MeV α + ^{61}Ni reaction and considerably less for all other targets.

The uncertainty in our absolute cross sections is $\pm$10%; the relative uncertainty as a function of energy is shown by the error bars in the spectra.

III. RESULTS AND PHENOMENOLOGICAL DISCUSSION

A. α-induced reactions

Figure 1 shows inclusive γ-ray spectra for α particles incident at $E_{\rm lab}$ = 27 MeV on targets ^{61}Ni, ^{95}Mo, ^{124}Sn, and ^{181}Ta. Also shown in Fig. 1 are statistical model calculations using a modified version of the code CASCADE [4], incorporating the GDR into the γ-ray strength function.

In all figures of spectra, the measured spectra are displayed along with calculated spectra which have been folded

TABLE I. Properties of studied reactions.

E_{lab} (MeV)	Reaction	S[a] (MeV)	E^*[b] (MeV)	$(E_{c.m.}-V_C)/A$[c] (MeV/u)
27.0	^{3}He+ ^{61}Ni		42.4	5.6
	^{95}Mo	2.75 ± 0.12	41.6	4.5
	^{124}Sn		41.4	3.9
27.0	^{3}He+ ^{148}Sm	2.31 ± 0.10	36.3	2.9
	^{181}Ta		37.1	2.1
16.0	^{3}He+ ^{62}Ni	1.86 ± 0.14	29.3	2.2
27.0	α+ ^{61}Ni		29.3	4.1
	^{124}Sn		29.3	2.9
	^{95}Mo	1.63 ± 0.12	28.1	3.3
28.0	α+ ^{119}Sn		28.6	3.2
14.9	^{3}He+ ^{96}Mo		29.3	0.6
15.9	^{3}He+ ^{120}Sn		28.6	0.3
27.0	α+ ^{154}Sm	1.58 ± 0.04	27.0	2.2
27.0	α+ ^{148}Sm	1.40 ± 0.04	24.2	2.2
	^{181}Ta		24.2	1.6
23.0	α+ ^{124}Sn	1.6 ± 0.3	25.4	2.0
20.0	α+ ^{124}Sn	1.5 ± 0.3	22.5	1.2
17.0	α+ ^{124}Sn	1.0± 0.3	19.6	0.5
11.0	^{3}He+ ^{62}Ni	1.60 ± 0.20	24.2	0.4
36.0	^{6}Li+ ^{98}Mo[d]	2.0 ± 0.2	46.8	2.6
	^{181}Ta[d]	1.5 ± 0.3	41.7	0.9

[a]Exponential shape factor determined for $E_\gamma > E_D$, characteristic of the reactions grouped between the horizontal lines.
[b]Excitation energy of combined system, before decay.
[c]Projectile energy minus Coulomb barrier energy, per incident nucleon.
[d]Reference [5].

with the measured line shape and efficiency. The absolute cross section scales shown on the ordinates of these figures have been deduced assuming a constant detector efficiency equal to that at E_γ=15.1 MeV. A close approximation to the true cross section can be obtained by dividing the displayed data by the energy-dependent efficiency factor $\exp[(E_\gamma-15)/32.7]$ above E_γ=15 MeV. This procedure neglects the effect of the shape of the response function, which is reasonable since the resolution is very good and the tail is small. Figures which show only spectra come from measurements at $\theta_\gamma=90^o$, and the absolute cross sections have been deduced assuming an isotropic angular distribution. Figures which contain fitted angular distribution coefficients (see Secs. III E and III F) display the total cross section determined from the fits.

Calculations using CASCADE have been generally successful in describing the γ-ray yield from heavy ion reactions at somewhat higher excitation energies [1]; details of the present calculations are given in Sec. IV A. For $E_\gamma<10$ MeV the statistical model reproduces the measured spectra well: the steep rise in cross section with decreasing E_γ is due to

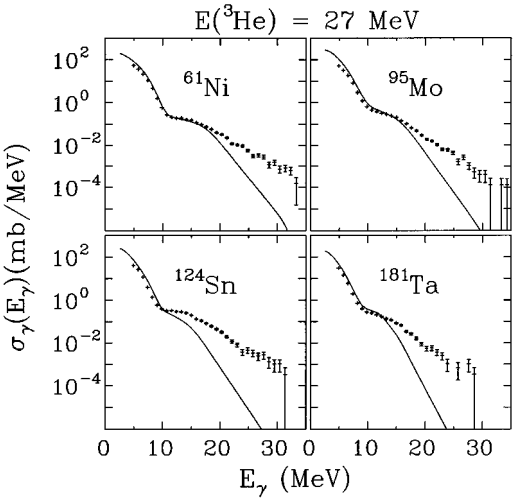

FIG. 2. Inclusive γ-ray production cross sections deduced from γ-ray spectra measured at $\theta_\gamma=90°$, and CASCADE calculations, for ^{3}He+ ^{61}Ni, ^{95}Mo, ^{124}Sn, and ^{181}Ta at $E(^3\text{He})=27$ MeV.

γ decays of residual nuclei which are populated by particle evaporation to within one nucleon binding energy of the yrast line. For the present reactions the statistical calculations for $E_\gamma > 15$ MeV are uncertain by a factor of less than 2, due to uncertainties in the width of the giant resonance built on excited states and in the level density at these low excitation energies. This is discussed further in Sec. IV A.

The statistical model can account for essentially the entire spectrum for the α+ ^{61}Ni reaction, consistent with earlier studies of 24 MeV α+ ^{59}Co [5] and 28 MeV α + ^{48}Ti [6]. For the heavier mass targets, the γ yield for $E_\gamma > 20$ MeV is 1 to 3 orders of magnitude greater than the statistical model calculation. Qualitatively, the ratio of the experimental yield to the statistical model calculation increases with target mass, although the absolute yield does not follow a monotonic trend with mass. Also, γ rays have been observed at energies $E_\gamma \approx E^*$, the compound nucleus excitation energy, where $E^* = Q + E_{c.m.}$ and $E_{c.m.}$ is the projectile energy in the center of mass—see Table I.

B. ^{3}He-induced reactions

In Fig. 2 are spectra for E_{lab} = 27 MeV ^{3}He incident on the same targets. Again, the spectra at low E_γ are consistent with the statistical model. The spectra for $E_\gamma > 15$ MeV greatly exceed the statistical model calculation for all target masses. The Q values for the ^{3}He-induced reactions are ~ 10 MeV greater than for the α-induced reactions, and finite yields are observed up to $E_\gamma \sim 35$ MeV, which is within 5–7 MeV of E^*, the kinematic end point.

The ^{3}He-induced cross-sections for $E_\gamma > E_D$, the GDR centroid energy, are considerably greater than the α-induced cross sections at the same E_γ for the same targets. This is expected for the simplest nonstatistical processes such as direct and semidirect $E1$ emission, which are suppressed for the $N=Z$ α particle. However, the higher Q values for the ^{3}He-induced reactions make this projectile dependence of the cross sections difficult to interpret; as we will see below, the higher cross sections may be partly a

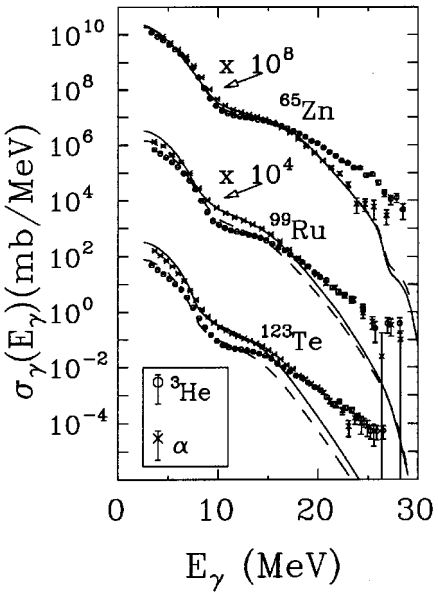

FIG. 3. Inclusive γ-ray production cross sections deduced from γ-ray spectra measured at $\theta_\gamma = 90°$, and CASCADE calculations, for reactions which form three different compound nuclei each with different entrance channels: 26.9 MeV α + ^{61}Ni and 16.0 MeV ^{3}He + ^{62}Ni, forming ^{65}Zn at $E^* = 29.3$ MeV; 27.0 MeV α + ^{95}Mo and 14.9 MeV ^{3}He + ^{96}Mo, forming ^{99}Ru at $E^* = 28.2$ MeV; and 28.0 MeV α + ^{119}Sn and 15.9 MeV ^{3}He + ^{120}Sn, forming ^{123}Te at $E^* = 28.5$ MeV.

result of the greater energy available in the ^{3}He-induced reactions, particularly if the reaction mechanism is more complex than direct plus semidirect.

C. Comparison of different reaction channels forming the same compound system

To investigate the role of the Q value in the reaction mechanism, we compared γ-ray yields from the same compound system produced at the same excitation energy with both ^{3}He and α entrance channels. The measured reactions are 16.0 MeV ^{3}He + ^{62}Ni and 27.0 MeV α + ^{61}Ni forming ^{65}Zn at $E^* = 29.3$ MeV; 14.9 MeV ^{3}He + ^{96}Mo and 27.0 MeV α + ^{95}Mo forming ^{99}Ru at $E^* = 28.2$ MeV; and 15.9 MeV ^{3}He + ^{120}Sn and 28.0 MeV α + ^{119}Sn forming ^{123}Te at $E^* = 28.5$ MeV. The absolute cross sections are displayed in Fig. 3, along with statistical model calculations. For these reaction pairs the statistical spectrum shape should be essentially the same, since the CASCADE calculations indicate that the difference in angular momentum distributions for the two entrance channels makes very little difference in the calculated γ-ray spectrum shape: the differences in magnitude of the statistical calculations are primarily due to differences in fusion cross section. Indeed, the experimental yield for $E_\gamma < 13$ MeV does scale with the statistical calculation; this is consistent with a statistical reaction mechanism as the primary source of these lower-energy γ rays.

The α + ^{61}Ni yield can be completely accounted for by the statistical model. The absolute yield for $E_\gamma \geq 18$ MeV is greater for ^{3}He + ^{62}Ni than for α + ^{61}Ni, implying a projectile dependence in addition to just the Q-value difference.

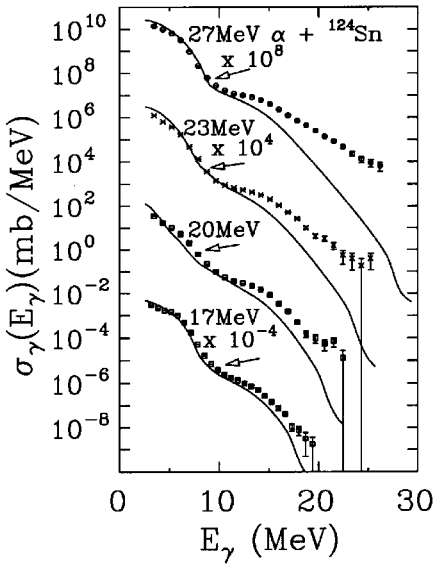

FIG. 4. Inclusive γ-ray production cross sections deduced from γ-ray spectra measured at $\theta_\gamma = 90°$, and CASCADE calculations, for α + ^{124}Sn at $E(\alpha) =$ 17, 20, 23.2, and 27 MeV.

In contrast, the absolute yields for $E_\gamma \geq 15$ MeV are almost identical for the two different entrance channels for the reactions on the Mo targets and for the reactions on the Sn targets. However, it is not clear whether this similarity in yield follows from some simple aspect of the reaction mechanism or whether it is an accident, since for these heavier targets, the ^{3}He bombarding energy is near the Coulomb barrier. In fact, if one were to correct approximately for the effect of the barrier by normalizing the curves in Fig. 3 to the same low-energy yield, which is essentially normalizing to the total reaction cross section, then the high-E_γ yield in the ^{3}He channel would again be larger. Thus it is difficult to

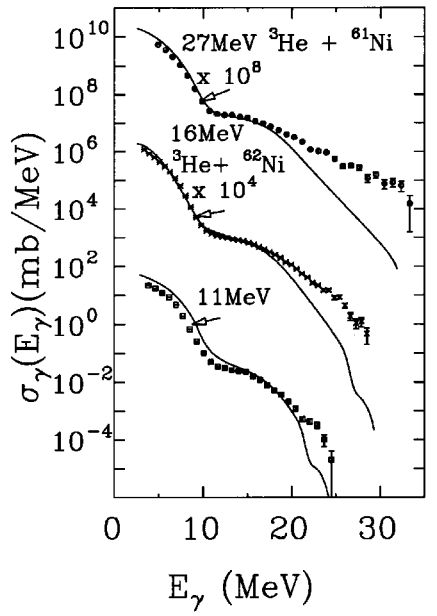

FIG. 5. Inclusive γ-ray production cross sections deduced from γ-ray spectra measured at $\theta_\gamma = 90°$, and CASCADE calculations, for ^{3}He + ^{61}Ni at $E(^{3}\text{He}) =$ 27 MeV, and ^{3}He + ^{62}Ni at $E(^{3}\text{He}) =$ 16 and 11 MeV.

interpret these results without a model for the nonstatistical reaction mechanism.

D. Dependence on projectile energy

We have also measured the dependence of the γ-ray yield on the projectile energy for a given target. Figure 4 shows spectra from α particles incident on ^{124}Sn at 17, 20, 23.2, and 27 MeV, and demonstrates that the discrepancy between the data and the statistical calculation increases as a function of projectile energy. For the lowest energy, $E_\alpha = 17$ MeV, the discrepancy is sufficiently small that with further adjustments of parameters, the statistical model might fit the data.

Figure 5 shows the spectrum from ^{3}He on ^{62}Ni at 11 MeV along with spectra already shown for ^{3}He on ^{62}Ni at 16 MeV and on ^{61}Ni at 27 MeV. Again at the lowest bombarding energy, $E_{^3\mathrm{He}} = 11$ MeV, most of the spectrum is reproduced by the statistical model calculation. At the higher projectile energies the measured yield is clearly in excess of the statistical model calculation at the higher γ-ray energies. These results may be compared to earlier studies in which the γ-ray spectrum from 11.8 MeV ^{3}He + ^{25}Mg ($E^* = 33.8$ MeV) was fitted with the statistical model [7].

E. Angular distributions

To further explore the nonstatistical nature of the reaction mechanism, we measured angular distributions of the emitted γ rays produced in the reactions 27 MeV α + ^{95}Mo, ^{148}Sm, and ^{154}Sm, as well as 27 MeV ^{3}He + ^{148}Sm. Inclusive spectra were measured at 40°, 90°, and 140° in the lab. Differential cross sections in the lab were converted to cross sections in the nucleus-nucleus center of mass frame by the formulas

$$\frac{d^2\sigma(\theta,E_\gamma)}{d\Omega dE_\gamma} = \gamma(1-\beta\cos\theta_L)\frac{d^2\sigma_L(\theta_L,E_{\gamma L})}{d\Omega_L dE_{\gamma L}}, \qquad (1)$$

$$E_\gamma = \gamma(1-\beta\cos\theta_L)E_{\gamma L},$$

$$\cos\theta = \frac{\cos\theta_L - \beta}{1-\beta\cos\theta_L},$$

where the subscript L denotes the lab frame and quantities without subscripts are in the center of mass frame. For these reactions, the lab to center of mass conversions are small, for example, $\beta_{\mathrm{c.m.}} = 0.005$ for $\alpha + ^{95}$Mo, affecting the extracted a_1 and a_2 by less than 0.1 for $E_\gamma \geq 15$ MeV. To obtain cross-section values at the same E_γ in the center of mass for different angles, spectra were interpolated.

The resulting spectra, binned in energy bins of ~ 1 MeV, were used to determine the coefficients of the Legendre polynomial expansion:

$$W(\theta) = 4\pi A_0[1 + a_1 P_1(\cos\theta) + a_2' P_2(\cos\theta)]. \qquad (2)$$

Since $P_3(\cos 40^\circ) \approx 0$, and $P_3(\cos 90^\circ) = 0$, we are not sensitive to a_3 and can neglect it. It is reasonable to neglect a_5, since a finite a_5 would require radiation of multipolarity 3, which probably is not large at these γ-ray energies. Thus a_1 as defined by Eq. (2) is a close approximation to the a_1 that would be obtained from a complete Legendre expansion of data taken at more angles. If $a_4 \neq 0$, then a correction for a_2 can be calculated: $a_2'(\mathrm{measured}) \approx a_2(\mathrm{true}) - (0.788)\, a_4(\mathrm{true})$. The results are shown in Figs. 6 and 7.

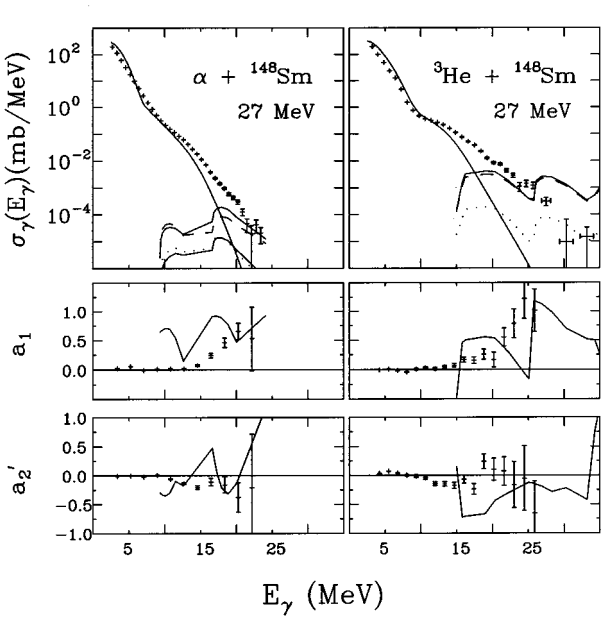

FIG. 6. Inclusive γ-ray production cross sections, CASCADE calculations, and a_1 and a_2' coefficients for α and ^{3}He + ^{148}Sm at $E(\mathrm{lab}) = 27$ MeV. The curves at high E_γ are direct-semidirect calculations: solid, total direct-plus-semidirect; dash, direct. Other curves for α: dot, Coulomb-induced semidirect; lowest solid, isoscalar semidirect. Other ^{3}He curve: dot, isovector semidirect.

For all our reactions, the a_1 coefficient is finite and positive for $E_\gamma \geq E_D$; i.e., the radiation is forward peaked in the center of mass frame. The fact that $a_1 \neq 0$ implies that there must be coherent interference between multipoles of oppo-

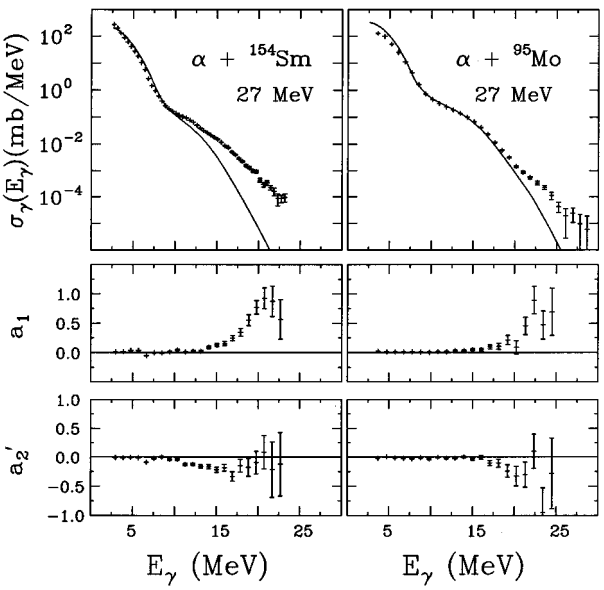

FIG. 7. Inclusive γ-ray production cross sections (with CASCADE calculations) and a_1 and a_2' coefficients for $\alpha + ^{154}$Sm and, ^{95}Mo at $E(\alpha) = 27$ MeV.

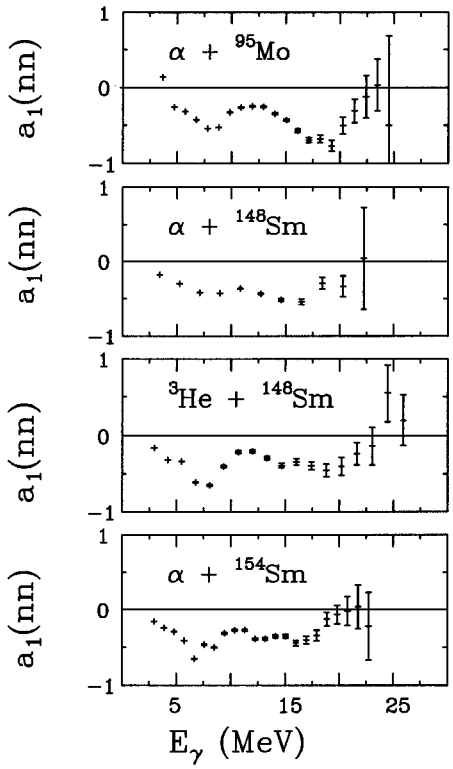

FIG. 8. a_1 coefficients transformed to the nucleon-nucleon center of mass frame. From top to bottom: $\alpha+{}^{95}$Mo, $\alpha+{}^{148}$Sm, ^{3}He + ^{148}Sm and $\alpha+{}^{154}$Sm, all at $E(\alpha)=27$ MeV.

site parity. We will see in Sec. IV that the qualitative behavior of the measured a_1 is consistent with direct radiative capture of $E1$ and $E2$ multipolarities. The fact that a_1 is so large near the end point energy implies that the $E1$ and $E2$ amplitudes are comparable at the highest γ-ray energies.

These results provide model-independent evidence for a reaction mechanism different from statistical decay of an equilibrated system. This follows from the fact that opposite parity radiations populating a given final state must come from opposite parity, and hence different, compound states. The assumption in the statistical model of phase incoherence among different compound states implies that such interference averages to zero. Thus statistical emission from the initial compound nucleus or its daughters must produce a front-back symmetric angular distribution in the nucleus-nucleus center of mass, and hence our observed deviations from front-back symmetry imply a nonstatistical reaction mechanism.

The value of E_γ for which a_1 becomes nonzero is lower for $\alpha+{}^{148}$Sm and $\alpha+{}^{154}$Sm than for $\alpha+{}^{95}$Mo, which may be due simply to the fact that statistical emission extends to higher E_γ in the lighter systems. At the lower γ-ray energies $E_\gamma<E_D$, $a_1\approx 0$ in the c.m. frame (Figs. 6 and 7). This suggests that the low-E_γ radiation is due to statistical emission from an equilibrated system. This conclusion is supported by the agreement between the measured cross sections and the CASCADE calculations for $E_\gamma < E_D$.

The interpretation of the a_2' coefficient is not as straightforward. In these reactions it is consistently less than zero at γ-ray energies near the giant dipole. The results are qualitatively consistent with direct-semidirect radiative capture (see Sec. IV); however, a negative a_2 can also be produced by spin plus deformation effects in statistical decay [1].

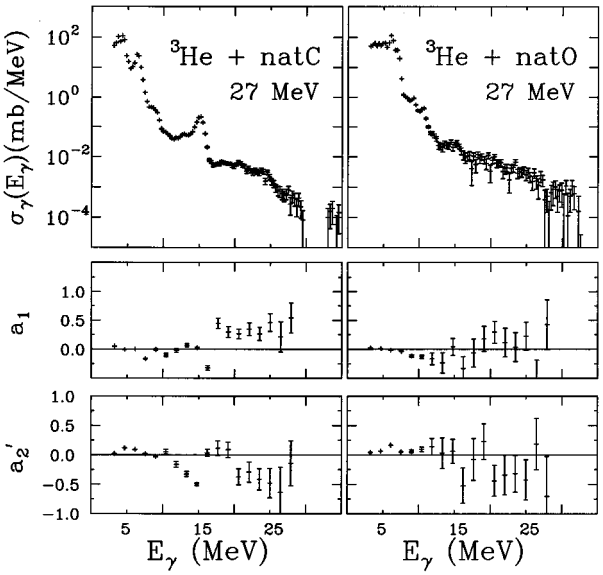

FIG. 9. Inclusive γ-ray production cross sections deduced from γ-ray spectra measured at $\theta_\gamma=90°$, and a_1 and a_2' coefficients for ^{3}He + natural C and natural O, at $E(^3\text{He})=27$ MeV.

A mechanism which has been successful in explaining the origin of the γ rays with $E_\gamma > E_D$ seen in medium-energy heavy ion collisions is incoherent bremsstrahlung, primarily from first neutron-proton collisions [2]. The usual approximation involves assuming only $E1$ radiation in the emitting frame; as a result, the cross section in this frame, which moves with approximately half the beam velocity, is forward-backward symmetric. For our reactions, in which the target is heavier than the projectile, the result is positive a_1 coefficients and hence forward peaking in the nucleus-nucleus center of mass.

To test whether this mechanism might be relevant to our reactions, we have transformed our cross sections to a reference frame moving with half the beam velocity, and fitted them to a Legendre polynomial expansion as before. The results for the a_1 coefficient for the $\alpha+{}^{95}$Mo, ^{148}Sm, and ^{154}Sm and ^{3}He$+{}^{148}$Sm reactions are shown in Fig. 8. The low-E$_\gamma$ part of the spectra is not symmetric about $\theta_\gamma=90^\circ$ in this frame [i.e., $a_1(nn)$ is not zero] since compound nuclear decay should be symmetric about $\theta_\gamma=90^\circ$ only in the nucleus-nucleus c.m. frame. For the three reactions on Sm, the statistical component is small above $E_\gamma \approx 16$ MeV, and in this region it is clear that in this frame, the nonstatistical emission is not symmetric about $\theta_\gamma=90^\circ$. This implies that, for these reactions, incoherent n-p bremsstrahlung is not the primary source of the observed γ rays, except possibly for the very highest γ-ray energies. In fact, for these reactions no frame exists for which $a_1=0$ for all $E_\gamma > 16$ MeV. For $\alpha+{}^{95}$Mo, the statistical contribution is small only at the highest E_γ, where $a_1(nn) \approx 0$ as in the other reactions.

We can conclude from the angular distributions and the failure of the statistical model to fit the spectra mentioned above that nonstatistical emission occurs for 27 MeV ^{3}He on

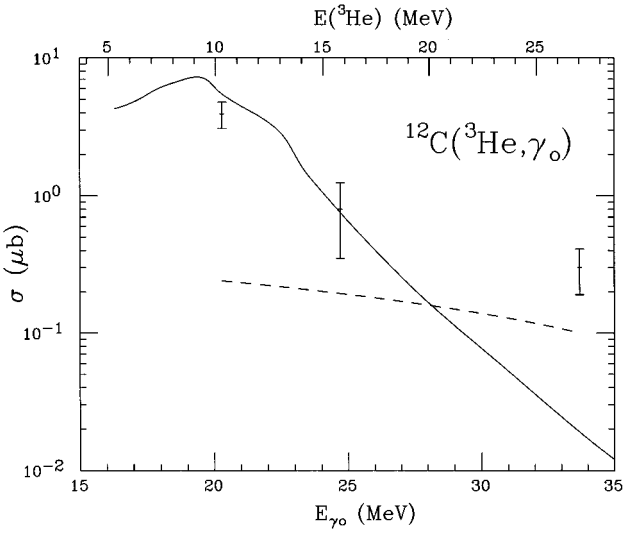

FIG. 10. Excitation function for the ^{12}C(^{3}He,γ_0)^{15}O reaction. Top axis is ^{3}He lab energy, bottom axis is γ-ray energy. Solid curve is statistical model, dashed curve is direct capture.

all targets, and becomes significant for 27 MeV α on targets comparable in mass to or heavier than Mo.

F. ^{3}He reactions on C and O

We have also measured angular distributions for reactions of 27 MeV ^{3}He + natural C (98.9% ^{12}C) and natural O (99.8% ^{16}O), which have total energy $E^*=$ 33.7 and 31.2 MeV, respectively. The results in the nucleus-nucleus center of mass frame are shown in Fig. 9. The large peak in the ^{3}He+C spectrum is from the 15.1 MeV $J^\pi=1^+$, $T=1$ state in ^{12}C formed by the ^{13}C(^{3}He,α)^{12}C* reaction, and perhaps by ^{12}C(^{3}He,^{3}He$'$). This state decays 88% by γ_0 emission [8]. Since γ emission from higher-lying states in ^{12}C formed in this reaction must compete with proton decay, and thus their γ-decay branches are suppressed by $\sim 10^3$ or more, the observed yield for $E_\gamma > 15.1$ MeV probably does not have significant contributions from inelastic scattering. The angular distributions are similar in character to those from the heavier targets, with positive a_1 at high E_γ and negative a_2' at E_γ near E_D, although the results for the ^{3}He + natural O reaction have marginal statistical significance. Finite cross sections extending to $E_\gamma = E^*$ are observed in both cases, with the γ_0 transition in the ^{12}C(^{3}He,γ) reaction clearly separated from other transitions by the 5.2 MeV energy of the first excited state of ^{15}O.

In Fig. 10 we show the ^{12}C(^{3}He,γ_0)^{15}O(g.s.) cross section measured at three energies. Also shown is a CASCADE statistical calculation of this cross section, with $E_D=21$ MeV and $\Gamma = 6$ MeV for the $T_<$ component of the GDR [9,10], and a direct capture calculation (see Sec. IV). These results indicate a reaction mechanism which changes from predominantly statistical at low projectile energy to predominantly direct at high projectile energy.

G. Effective charges for direct capture

The observed target mass dependence of the nonstatistical yields suggests that the $E1$ effective charge q_{E1} may play a role in the nonstatistical emission rate. The effective charge for radiation of multipolarity L is given by

$$q_{EL}=\mu^L\left(\frac{Z_p}{A_p^L}+(-1)^L\frac{Z_t}{A_t^L}\right) \tag{3}$$

where p and t subscripts denote projectile and target, and μ is the reduced mass.

TABLE II. $E1$ and $E2$ effective charges for studied reactions.

Target	q_{E1}^2		q_{E2}^2	
	α	^{3}He	α	^{3}He
^{61}Ni	0.024	0.35	3.5	3.5
^{62}Ni		0.38		3.5
^{95}Mo	0.049	0.43	3.7	3.7
^{96}Mo		0.44		3.7
^{119}Sn	0.10		3.7	
^{120}Sn		0.54		3.7
^{124}Sn	0.14	0.60	3.7	3.7
^{148}Sm	0.10	0.53	3.8	3.8
^{154}Sm	0.14		3.8	
^{181}Ta	0.14	0.60	3.8	3.8

The cross sections for $E1$ and $E2$ direct radiative capture are proportional to the squares of q_{E1} and q_{E2}, respectively. The $E1$ effective charge is zero for an α incident on an $N=Z$ target, since the dipole moment in the center of mass vanishes. For the α-induced reactions studied here, the square of q_{E1} increases by an order of magnitude from the lightest to the heaviest target mass, while it is relatively constant and much larger for the ^{3}He-induced reactions (Table II). This is qualitatively consistent with the observed trends of the nonstatistical yields.

A more direct test can be made by comparing 27 MeV $\alpha+^{154}$Sm with 27 MeV $\alpha+^{148}$Sm (Fig. 11) in the region above $E_\gamma = 18$ MeV, where the statistical yield is small. For this reaction pair, the ratio of q_{E1}^2 for the two different target isotopes is approximately 1.4 (Table II), while the other reaction properties which affect direct (and semidirect) emis-

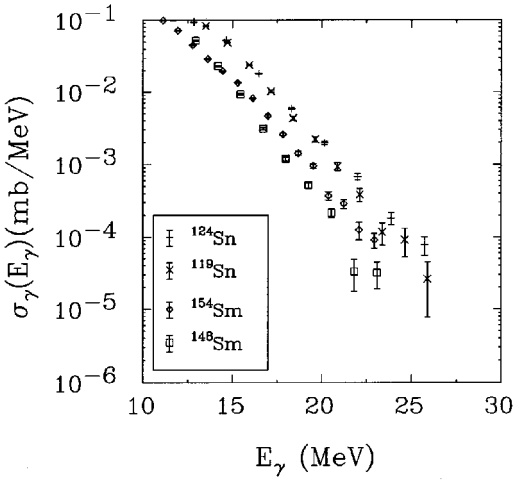

FIG. 11. Comparison of inclusive γ-ray production cross sections for $\alpha+^{119}$Sn at $E(\alpha)=28$ MeV, and $\alpha+^{124}$Sn, ^{148}Sm, and ^{154}Sm at $E(\alpha)=27$ MeV.

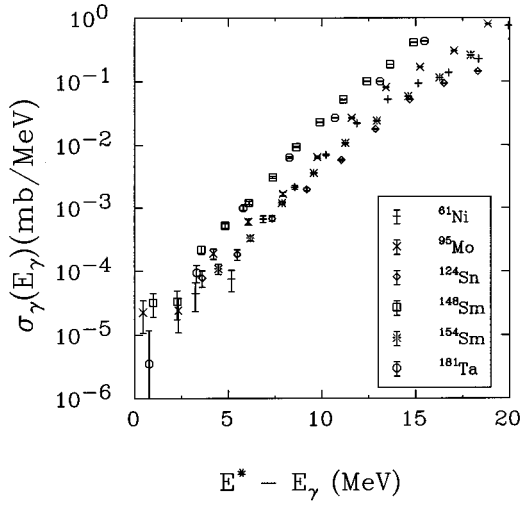

FIG. 12. Comparison of γ-ray production cross sections plotted as a function of E^*-E_γ, for 27 MeV α + ^{61}Ni, ^{95}Mo, ^{124}Sn, ^{148}Sm, ^{154}Sm, and ^{181}Ta.

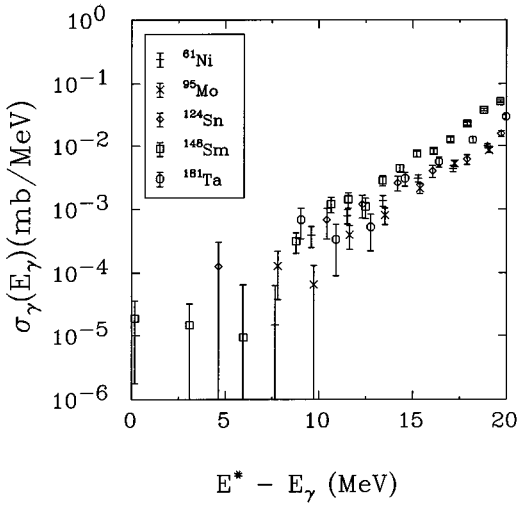

FIG. 13. Comparison of γ-ray production cross sections plotted as a function of E^*-E_γ, for 27 MeV ^{3}He + ^{61}Ni, ^{95}Mo, ^{124}Sn, ^{148}Sm, and ^{181}Ta.

sion such as Q values and distorted waves are very similar. In the high-energy region, the $\alpha+^{154}$Sm cross section is somewhat larger than the $\alpha+^{148}$Sm cross section, as expected from the $E1$ effective charges. One may also compare 27 MeV $\alpha+^{124}$Sn with 28 MeV $\alpha+^{119}$Sn (Fig. 11). Here the q^2_{E1} ratio is the same as for the Sm reactions. The high-E_γ cross section ratio for the Sn reactions is approximately unity. The measured projectile energy dependence (Fig. 4) suggests that this same ratio for Sn reactions, both at 27 MeV, would be somewhat greater than unity. Although the trend of these cross sections follows q^2_{E1}, we should not expect close numerical agreement since near the end points, $E1$ and $E2$ contributions are probably comparable (see Sec. IV B).

H. Yield correlations with E^*

There appears to be a correlation between the observed yields and the total energy E^* available in the reaction. For all targets, the spectra at $E_\alpha = 27$ MeV show a correlation with E^* in both slope and magnitude. In Table I are compiled exponential slopes S that describe the nonstatistical high-energy region of the various spectra, where $\sigma_\gamma = \sigma_0 \exp(-E_\gamma/S)$. For ^{3}He-induced reactions and, separately, for α-induced reactions, spectra with a similar E^* have a similar slope. In particular, the yields from 27 MeV $\alpha+$ ^{61}Ni, ^{95}Mo, and ^{124}Sn, and 28 MeV $\alpha+^{119}$Sn all have similar slopes and, in fact, similar magnitudes, and they all have $E^* \approx 28$ MeV. These systems differ in q^2_{E1} by a factor of 6. The yields from $\alpha+^{148}$Sm and ^{181}Ta, which both have $E^* \approx 24$ MeV, also group together. The nonstatistical yield from $\alpha+^{154}$Sm falls in between these two groups in E^*, magnitude, and slope. Similar groupings also exist for the ^{3}He-induced reactions, with slopes that are quite different from those for the α-induced reactions. In spite of these arguments, one should treat the apparent correlations with E^* with caution. Other extensive variables, notably $(E_{\text{c.m.}}-V_C)/A$, the bombarding energy above the Coulomb barrier, vary systematically over the present data set and may be responsible for some of the observed behavior.

Other interesting phenomenology can be obtained by extrapolating the high-energy yields to obtain the cross section near the total energy available, $\sigma(E_\gamma \approx E^*)$. This quantity is very similar for all of the α-induced reactions, and separately for all of the ^{3}He-induced reactions. This is best seen by comparing the cross sections as a function of the energy away from the end point, $\sigma(E^*-E_\gamma)$, as shown in Figs. 12 and 13. Although the characteristic slopes of the α-induced spectra are quite different from those of the ^{3}He-induced spectra, $\sigma(E_\gamma \approx E^*)$ for the ^{3}He-induced reactions is within a factor of 2 of $\sigma(E_\gamma \approx E^*) \approx 10^{-5}$ mb/MeV for the α-induced reactions. Thus the yield and slope of the high-energy tail of γ rays appears to be largely determined by the total energy available in the reaction, for either the α- or the ^{3}He-induced reactions.

In order to explore these issues more quantitatively, we have calculated the γ-ray emission rate for several specific processes, as discussed in the following section.

IV. CALCULATIONS AND DISCUSSION

We calculate two distinct extremes of radiative reaction mechanisms. One is the γ-ray yield due to statistical emission from an equilibrated compound system, which is dominated by decays of the GDR. At the other extreme of complexity in the reaction dynamics, we calculate radiation from direct and semidirect processes, with the goal of determining whether the resulting magnitude and angular distribution can help explain the observed nonstatistical high-energy yield. We have performed distorted wave calculations of direct semidirect (DSD) radiation— radiation from direct radiative capture and from semidirect (single-step) excitation of the GDR— patterned after those done in the literature for (p,γ) reactions [11] and for (α,γ_0) reactions on light nuclei [12]. By extending the DSD formalism, we have also crudely estimated the radiation emitted by exciting the GDR in the projectile. All of our calculations of nonstatistical γ emission assume that the projectile maintains its integrity during the capture process.

A. Statistical model calculations

In order to quantify the contribution from statistical emission, we have used the code CASCADE . The use of this code to model statistical γ-ray production is well established [1]; we will describe a few of the relevant details here.

The width for $E1$ statistical decay is given by [1]

$$(d\Gamma_\gamma/dE_\gamma)_J = \sum_{J_f=J,J\pm1} \frac{\rho(E^*-E_\gamma,J_f)}{\rho(E^*,J)} \frac{\sigma_{\rm abs}(E_\gamma)}{3} \frac{E_\gamma^2}{(\pi\hbar c)^2} \tag{4}$$

where $\sigma_{\rm abs}(E_\gamma)$ is the total photoabsorption cross section for a state at excitation energy (E^*-E_γ) with spin J_f.

We approximate the effective photoabsorption cross section to be a single-Lorentzian GDR. From previous work on heavy ion reactions, we can restrict the parameters of the GDR built on excited states [1]. We take the dipole strength equal to one Thomas-Reiche-Kuhn sum rule, and E_D equal to the centroid energy of the dipole resonance built on the ground state, as given by experimental photoabsorption systematics [13] ($E_D = 31.2A^{-1/3}+20.6A^{-1/6}$). The width is not known *a priori*, but since the spin and temperature of the final states on which the GDR is built are lower than in previous heavy ion work [1], we estimate $\Gamma=7$ MeV, and we used this value in all our calculations except for ^{12}C(^{3}He, γ_0) ^{15}O.

It has been suggested [14] that the photoabsorption cross section used in Eq. (4) should include, in addition to the GDR, some part of the quasideuteron process, because the quasideuteron is more likely to be absorbed and form a compound nucleus in a system with a high temperature. If the total photoabsorption cross section, including the quasideuteron tail, were used in Eq. (4), then the γ-ray cross section at 30 MeV would increase by no more than 30%. Since our nuclei are not nearly as hot as those in Ref. [14], which involves temperatures as high as 6 MeV, this is certainly an overestimate; in any case this will not qualitatively affect the present results. The giant quadrupole resonances (GQR's) have not been included in these calculations. The main effect is from the isovector GQR, which increases the cross section at 32 MeV, the highest γ-ray energy, by up to 40%.

One of the largest uncertainties in the calculation is the dependence on the level density. We are always concerned with $\Gamma_\gamma/\Gamma \approx \Gamma_\gamma/\Gamma_{\rm particle}$, and $\Gamma_{\rm particle}$ has a dependence on ρ_i and ρ_f similar to that of Γ_γ [1]. So in the ratio of the widths, the factors of ρ_i cancel out, and we are only dependent on a ratio of final-state level densities for particle and γ emission.

We have used a level density parametrization due to Reisdorf and used in the statistical code HIVAP [15,16]; its use has been found to give a consistent picture of the level density in describing statistical γ decay in light nuclei $A=39-63$ [5,17,6], and it was also used to provide a consistent statistical model fit to 27 MeV $\alpha+^{59}$Co [5] and 27 MeV $\alpha+^{48}$Ti [6]. In this approach the level density function is given by

$$\rho(E,J) = \frac{2J+1}{12\Theta^{3/2}} \sqrt{a}\ \frac{\exp(2\sqrt{aU})}{U^2} \tag{5}$$

where

$$aU = \tilde{a}\{U+\delta U[1-\exp(-\gamma U)]\},$$

$$U = E+\delta P - J(J+1)/\Theta',$$

$$\Theta = 2I/\hbar^2,$$

$$\Theta' = \Theta(1+\delta J^2+\delta' J^4).$$

U is a free energy, δP and δU are backshifts for pairing and shell corrections, and $\tilde{a}$ and γ are constants. $I=2/5MR^2$ is the rigid-body moment of inertia, and Θ' includes corrections for a deformable liquid drop [18].

This formulation provides a physically plausible dilution of shell effects with increasing energy as the liquid drop regime is approached. This description provides a proper liquid drop level density in the limit of large U, and at the same time matches on average the level density at neutron threshold for $A=100$ to 250 [15] and for nuclei in the region of $A=60$ [5]. It thus provides a physically reasonable, smooth level density for all excitation energies, although it does not necessarily fit neutron threshold level densities for each individual case. We believe that use of the Reisdorf level density, for the relatively low excitation energies populated in these reactions, should provide a good determination of the statistical γ-ray yield.

From the comparisons discussed in Sec. III, we conclude that the statistical model can account for the high-energy γ-ray yield from 11 MeV ^{3}He+^{62}Ni, and 17 MeV $\alpha+$ ^{124}Sn, as well as from 27 MeV α-induced reactions on targets as heavy as ^{61}Ni. To reproduce the yield from 27 MeV α-induced reactions on ^{95}Mo we would have to set the GDR parameters to physically unrealistic extremes; we have already seen the forward-peaked angular distribution for this reaction indicating its nonstatistical nature. For 27 MeV α's on higher-mass targets we clearly cannot fit the high-energy spectra with the statistical model. For the 27 MeV ^{3}He-induced reactions we have large high-energy nonstatistical tails for all target masses.

B. Direct capture

Direct radiation is produced by the acceleration of the projectile in the mean field of the target. It is thus analogous to what is termed ''coherent bremsstrahlung'' [3] in medium-energy heavy ion collisions. Fermi's golden rule gives

$$\frac{d\sigma^2}{d\Omega dE_\gamma} = \frac{2\pi}{\hbar v_{\rm proj}} |\langle \psi_i | \mathcal{O}_{\rm EM} | \psi_f \rangle|^2 \frac{d\rho}{d\Omega}. \tag{6}$$

The target wave function is assumed not to change in the reaction, and factors out. The initial-state projectile wave function is taken to be the distorted wave in the optical model potential taken from scattering data. The final state is the bound state of the projectile moving in the real part of this optical potential. We use a version of the ABACUS code, as modified by T. Murakami, for calculating the wave functions and the radial matrix elements.

The bound final-state wave function is determined by a cluster model. The ground state in the final nucleus is bound at the desired energy (see below) by adjusting the well depth. The ground-state angular momentum is assumed to be that of

TABLE III. $\alpha+{}^{148}$Sm cluster levels in optical potentials used. The horizontal lines separate groups of states with the same $2N+L$.

N	L	E (MeV)[a]	E (MeV)[b]
6	9	unbound	17.1
5	11	unbound	15.1
10	0	14.7	13.9
9	2	14.6	13.7
8	4	14.4	13.1
7	6	14.0	12.1
6	8	13.4	10.7
5	10	12.6	8.7
4	12	11.5	6.1
9	1	7.5	6.9
8	3	7.2	6.4
7	5	6.8	5.5
6	7	6.2	4.1
5	9	5.3	2.2
4	11	4.1	<0.0
3	13	2.5	<0.0
9	0	0.0	0.0

[a]Potential of Ref. [28].
[b]Potential of Ref. [29].

the actual nucleus; we then determine the radial quantum number by a weak coupling assumption:

$$2N+L=\sum_{i=1} 2n_i+l_i \tag{7}$$

where N, and L are the radial and angular momentum quantum numbers of the center of mass of the He cluster in its orbit, and n_i and l_i are the quantum numbers of the nucleons making up the He moving in single-particle shell model orbits about the nuclear center of mass. This relation is exact for a cluster of nucleons moving in a relative $1s$ state in a common harmonic oscillator shell model potential with no residual interactions between the nucleons. It is simply obtained by equating the energy of the cluster center of mass with the summed energy of its individual nucleons. The center of mass coordinate separates from the relative coordinates of the cluster because the harmonic potential is proportional to r^2, and hence the quantum numbers of the separable motion are additive [19]. This procedure yields, for example, a ground-state wave function with eight-nodes for an α particle bound in ^{128}Te.

The possible excited cluster states in the final nucleus which may be populated in the capture process are then determined by fixing the well depth and finding the excited states that result, both with the same and with higher $2N+L$. Most of the final states that contribute to capture in the energy region of interest are physically located in the continuum. To simplify the model calculation, we artificially bind the ground state deep enough so that the final states of interest are bound in the well. We are only interested in states that lie below the Coulomb barrier for helium emission, which makes this approximation reasonable. Table III shows the resulting level schemes for α states bound to ^{148}Sm for the two different optical potentials that we considered (see below); for these schemes we artificially bound the ground state by an extra 20 MeV. Such calculated level schemes provide only a rough guide to the approximate energy of α spectroscopic strength of particular N and L relevant to our experiments.

The energy dependence of the resulting α level density is quite flat, consistent with what one would estimate from single-particle states in a harmonic oscillator. There are a total of $(2N+1)$ levels lying in energy between $2N\hbar\omega$ and $(2N+2)\hbar\omega$, so the density of such single-particle levels is $(2N+1)/(2\hbar\omega)$. This density changes only slowly with energy (i.e., with N). If we bind the ground state of the He + target nucleus system at an energy of 0 MeV, then $2N\hbar\omega \approx V_r$, the depth of the real potential. Then the density of single-particle levels is $\rho_{\mathrm{He}}\approx V_r/2(\hbar\omega)^2$. This yields a cluster level density of ≈ 1 per MeV for $\alpha+$Sn and 1/2 per MeV for $\alpha+$Ti, for clusters with nucleons in a relative $1s$ state.

Such cluster model wave functions are commonly used to interpret α spectroscopic strength found from α transfer and pickup reactions [20–23] and α decay [24] and have also been used to describe detailed properties of α cluster states and spectra in nuclei as heavy as ^{44}Ti [25,26]. The average α level density in medium-mass nuclei is found experimentally from α transfer and pickup reactions to be essentially flat with energy up to 6 MeV excitation; a flat energy dependence is also consistent with β-delayed α emission studies [27]. A cluster model treatment for the final-states is not so well justified for ^{3}He. We use the cluster model approach with some confidence as an indication of the average final-state level density that looks like projectile + target, and we assume the spectroscopic factors $C^2S=1$.

The resulting calculated direct γ-ray cross sections and angular distribution coefficients for 27 MeV α and 27 MeV ^{3}He on ^{148}Sm are shown as dashed curves in Fig. 6. We have shown the cross sections populating the cluster states as determined above, connecting the cross sections to the individual cluster states with lines, and normalizing to the average number of states per MeV to determine the differential cross section per unit energy. The structure in the calculations is due to the location of these cluster states. Rather than draw a physically more reasonable smooth average curve through the calculations, we have chosen not to obscure the details of the calculation. These calculations include $E1$ and $E2$ multipolarities. We compute $a_2'=a_2-(0.788)a_4$, where a_2 and a_4 are calculated in the model, and compare directly to the data, as discussed in Sec. III E. The a_4 is substantial in our direct calculations.

To explore the sensitivity of the direct calculation to the optical model used, calculations for $\alpha+{}^{148}$Sm using two different optical potentials were done. The results are shown in Fig. 14. The solid curve uses a global optical model of Dabrowski and Freindl [28]. This optical model uses a Woods-Saxon squared function for the real potential, and was obtained from fits of α scattering at energies 90–172 MeV on targets of mass 12–208. Those data include large-angle ''rainbow scattering'' and thus this potential should be free from problems of discrete ambiguities in potential parameters associated with potentials derived from lower-energy scattering data. Because of the dependence of the $E1$ and

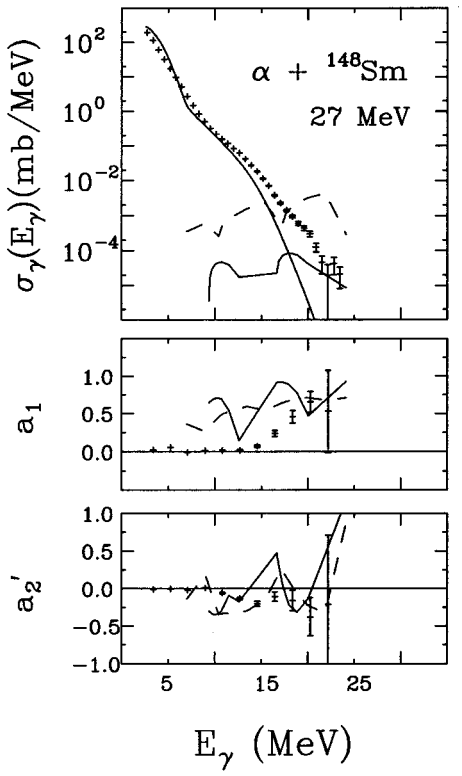

FIG. 14. Direct radiative capture calculations for 27 MeV α + ^{148}Sm. Solid, potential of Ref. [28]; dash, potential of Ref. [29]. Data are the same as Fig. 6.

$E2$ operators on r, the direct radiation calculation is sensitive to the interior of the potential; i.e., γ rays of these wavelengths see the whole nucleus. The dashed curve shows for comparison a calculation using an optical model of Aponik *et al.* [29], which fits scattering of 27.5–32.5 MeV α's on ^{148}Sm with a Woods-Saxon shape for the real part. Aponik *et al.* make no claims about this potential's uniqueness, and this calculation is included here to show the sensitivity of the magnitude of the calculation to the optical model chosen. Both these potentials have real well volume integrals close to the values suggested by studies of α-particle scattering which resolved the problem of discrete ambiguities [30].

An additional uncertainty in the absolute magnitude of the cross section comes from the need to artificially bind the ground state. If we bind the ground state by only an extra 10 MeV instead of 20 MeV, the calculated γ_0 cross section is twice as large.

The potential we use for ^{3}He is the global potential of Hyakutake *et al.*; it is also a potential derived from an analysis of data which should be free from discrete ambiguities [31]. It uses a Woods-Saxon for the real part and the first derivative of the Woods-Saxon (surface form) for the imaginary part. We bind the ground state by 10 MeV more than its physical depth of 9.8 MeV so that we can calculate transitions over the whole γ-ray energy range of interest. Thus the total binding energy used for the ground state in both the α-capture and ^{3}He-capture calculations is the same, about 20 MeV. Here again, if we bind the ground state by 10 MeV less than this, namely, at its physical depth of 9.8 MeV, the calculated γ_0 cross section is twice as large.

Although clearly the absolute magnitude of the calculated yield is uncertain, it can be concluded that direct radiative capture may dominate in both the ^{3}He- and α-induced reactions at the highest γ-ray energies. However, the calculated spectrum shapes are too flat to explain most of the experimental nonstatistical cross sections. This weak dependence of the cross section on γ-ray energy is determined by kinematic factors, the He cluster final-state level density, and the energy dependence of the radial integrals; the latter energy dependence is small and unchanging with optical model.

The calculated angular distribution is in qualitative agreement with experiment at the highest γ-ray energies, independent of the set of optical model parameters used (Fig. 14). The calculations suggest that the direct $E1$ and $E2$ amplitudes are approximately equal at the highest γ-ray energies for ^{148}Sm(α,γ), thus generating a large forward peaking which agrees with experimental observation.

C. Semidirect excitation of the target

Semidirect radiation arises from single-step excitation of the GDR in the entrance channel, which then radiates. The ^{3}He projectile has nonzero isospin and hence can excite the isovector GDR in such a single-step process; this is the dominant process in (p,γ) radiative capture at γ-ray energies near the GDR. In the naive semidirect model, this is the GDR in the target nucleus; however, it has been argued that within the framework of the semidirect approximation, it does not make sense to distinguish between the target GDR and the GDR in the combined system. In our heavy nuclei this is not an important distinction. The semidirect radiation can be calculated using the same distorted-wave formalism as for direct capture, by modifying the electromagnetic operator r^l to include a term involving a form factor $f(r)$ for the GDR excitation [32–34]. We use the Steinwedel-Jensen (S-J) or volume form factor, in which $f(r)$ has the same functional form as the mass density; we take this to be proportional to the optical potential [35]. Use of the Steinwedel-Jensen model instead of the Goldhaber-Teller (G-T) model has become common in semidirect radiative nucleon capture calculations. This is because the G-T form factor, which is proportional to the derivative of the optical potential, has an imaginary component that is the derivative of a surface-peaked function and hence contributes very little to the cross section, in apparent disagreement with the magnitude of observed cross sections for nucleon-induced radiative capture in heavy nuclei.

In order to include the semidirect radiation, we modify the radial operator by [36,32–34]

$$q_{E1}r \rightarrow q_{E1}r + \frac{F(r)}{E_\gamma - E_{\mathrm{D}} + i\Gamma/2} \tag{8}$$

where the semidirect factor F is given by

$$F(r) = -\frac{r}{\langle r^2_{\mathrm{tar}}\rangle}\frac{V_1(r)\tau_{3,\,\mathrm{proj}}}{E_{D,\mathrm{tar}}A_{\mathrm{tar+proj}}}\frac{NZ}{A}\frac{3\hbar^2}{4m_{\mathrm{proton}}}, \tag{9}$$

$$V_1(r) = 4Vv(r) + i16Wa_I\left|\frac{\partial w(r)}{\partial r}\right|.$$

Here $v(r)$ and $w(r)$ are the functional forms of the real and imaginary parts of the optical potential, normalized to unity at $r=R$, and a_I is the diffuseness of the imaginary potential.

We take the strength of the real coupling $V = 14.9$ MeV from the isovector term in the optical potential for the ^{3}He [31]. We take the strength $W \approx 7$ MeV for the imaginary coupling from the imaginary isovector optical potential term, which comes from (^{3}He,t) data [30]. Theoretical grounds for the use of the optical model depth for the coupling strength, based on folding model considerations, are quite good for the real part [35] but not so good for the imaginary part [35]; however, the imaginary part makes only a small contribution here, as shown below.

The results for the semidirect process are small. Figure 6 shows the coherent sum of the direct and semidirect processes, which is very similar to the direct alone. If one were to arbitrarily boost the coupling strengths in the semidirect form factors to match the magnitude of the data just above the GDR centroid, increasing the real or imaginary strength by a factor of order 20, then the calculated semidirect cross section would exceed the data at the highest γ-ray energies by a factor of 10. Hence the semidirect amplitude does not have a strong enough dependence on E_γ to explain the experimental spectra in the high-energy nonstatistical region.

The $T=0$ α cannot excite the GDR in a single-step process, except through the Coulomb potential, or by the isoscalar nuclear interaction if the ratio of neutron to proton densities is not proportional to the constant factor N/Z throughout the target. We have calculated both of these effects according to prescriptions of Satchler [35,37]. The form factor for Coulomb semidirect excitation [35] is obtained by replacing in Eq. (9):

$$rV_1(r)\tau_{3,\mathrm{proj}} \rightarrow \frac{-b}{r^2}, \quad r \geqslant R_c \tag{10}$$

$$\frac{-br}{R^3}, \quad r < R_c,$$

where $b = A_{\mathrm{tar}} R_c^2 Z_{\mathrm{proj}} e^2/10$, and R_c is the Coulomb charge radius. We have calculated the cross section from this semidirect process and found it to be smaller than but on the same order as the direct radiation. The results for $\alpha + {}^{148}$Sm are shown in Fig. 6 as the dotted curve. For an isoscalar excitation of the GDR, we make an estimate based on the schematic model. In this model the transition density for isovector excitation of the GDR is proportional to $r\rho(r)$ (the same form as is generally taken for the Steinwedel-Jensen model) where $\rho(r) = \rho_n(r) + \rho_p(r)$. The corresponding transition density for isoscalar excitation of the GDR is equal to [38]

$$\rho^{\mathrm{tr}}(r) = r\left(\frac{Z}{A}\rho_n(r) - \frac{N}{A}\rho_p(r)\right). \tag{11}$$

This transition density does not satisfy the constraint that the center of mass remain fixed for dipole oscillations, which implies that the integral over all space of the transition density should vanish [37]. If we arbitrarily add to this $\rho^{\mathrm{tr}}(r)$ a term to make its integral vanish,

$$\frac{NZ}{A^2}\frac{\langle r_n^2\rangle - \langle r_p^2\rangle}{\langle r^2\rangle} r\rho(r), \tag{12}$$

then we find our final γ-ray cross section from isoscalar GDR excitation increases by 25%, and our total direct-plus-semidirect cross section decreases by 10%. This suggests that properly including the center of mass constraint would have only a small effect on the result, so for our purposes we can safely ignore the center of mass constraint and use Eq. (11) for our transition density.

We use an ansatz for the differing neutron and proton densities used by Satchler [37]:

$$\rho_{n,p}(r) = \frac{1}{2}(1 \pm \epsilon x)\rho\left[r - c\left(1 \pm \frac{\gamma x}{3}\right)\right], \tag{13}$$

where $x = (N-Z)/A$, $\gamma x = (3/2)(\Delta R/R)$, $\epsilon = 1-\gamma$, and c is an average radius so that the neutron and proton radii are related by $c_{n,p} = c(1 \pm \gamma x/3)$. The $+$ is for neutron and $-$ is for proton. Assuming the same ansatz for the mean potentials due to the neutrons and protons, this leads in the Steinwedel-Jensen model to the form factor for isoscalar semidirect excitation, which is given by replacing in Eq. (9):

$$rV_1(r)\tau_{3\,\mathrm{proj}} \rightarrow \frac{3}{2}\frac{\Delta R}{R} r\left|\mathrm{V}_0(r) + \frac{1}{3}R\frac{dV_0(r)}{dr}\right| \tag{14}$$

where $V_0(r)$ is the central optical potential and R is its radius. For ΔR, the difference in rms radii between neutrons and protons, we take results from 1 GeV proton scattering data [39] as a guide, and choose $\Delta R = 0.13$ fm.

For 27 MeV $\alpha + {}^{148}$Sm, the Coulomb and isoscalar semidirect radiative amplitudes are roughly equal, and equal to about 1/3 of the amplitude for direct radiative capture (Fig. 6). The interference is constructive in the region of the GDR. However, including the semidirect radiation does not significantly alter the qualitative results from the calculation of direct radiation alone. The total direct-plus-semidirect cross section is still an order of magnitude smaller than the data in the region of the GDR, and its dependence on E_γ is still too flat to explain the data.

D. Semidirect excitation of the projectile

Given the assumption that the projectile maintains its integrity during the capture process, one can consider radiation produced from the one-step excitation of the GDR in the *projectile* by the isovector nuclear potential of the target. This mechanism is not isospin forbidden for the α projectile if the target has $N \neq Z$. We have very crudely estimated the yield from such a process using a formalism similar to the semidirect target excitation. The major complication is that the target cannot be treated as a point source.

The interaction potential is given by (ignoring exchange terms)

$$\Delta U(\vec{r}) = \int\int v_1(\vec{r'},\vec{r''})\rho^{\mathrm{tr}}_{\mathrm{proj}}(\vec{r''})\rho^{\mathrm{IV}}_{\mathrm{tar}}(\vec{r'}-\vec{r})d\vec{r'}d\vec{r''} \tag{15}$$

where both the transition density and the isovector density are proportional to the mass density $\rho(\vec{r})$:

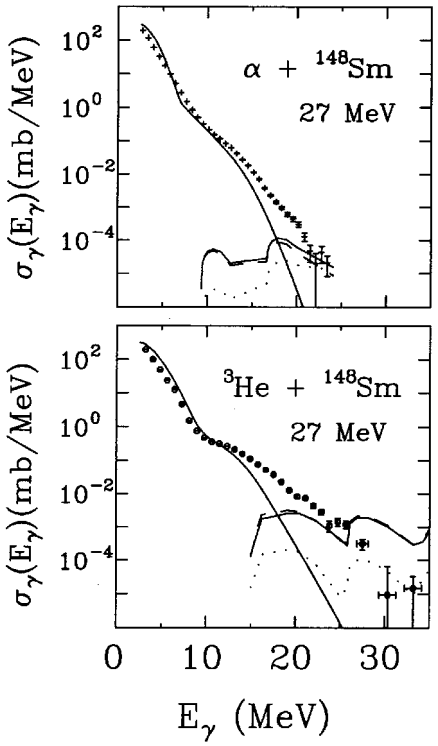

FIG. 15. Calculated yield from semidirect excitation of the projectile GDR: dot, projectile GDR excitation; dash, direct; solid, total direct+projectile GDR excitation. Data are the same as Fig. 6.

$$\rho^{\rm tr}_{\rm proj}(\vec{r''}) = \frac{K}{\sqrt{2L+1}} |\vec{r''}| \rho_{\rm proj}(\vec{r''}),$$

$$\rho^{\rm IV}_{\rm tar}(\vec{r'} - \vec{r}) = \frac{\tau_3}{A} \rho_{\rm tar}(\vec{r'} - \vec{r}),$$

$$K = \frac{8\pi}{A_{\rm proj}\langle r^2_{\rm proj}\rangle} \left(\frac{\hbar^2}{2m_{\rm proton}} \frac{3}{4\pi} \frac{NZ}{A} \right)^{1/2}_{\rm proj}.$$

For the purpose of this estimate, crude simplifying assumptions have been made; it is assumed that the target has uniform density over the region where the projectile is located, and that the contribution to the radial integral is only nonzero when the projectile is completely inside the target. Assuming the isovector two-body potential has zero range, one obtains

$$\Delta U(r) = \frac{V_1(0) K}{\sqrt{2L+1}} \frac{A_p \tau_{3,\rm tar}}{A_{\rm tar}} \rho_{\rm tar}(r) \langle r_{\rm proj}\rangle. \quad (16)$$

Our result for the semidirect form factor $F_{\rm proj}$ for exciting the GDR in the projectile is

$$F_{\rm proj}(r) = - \frac{\langle r_{\rm proj}\rangle}{\langle r^2_{\rm proj}\rangle} \frac{V_1(r)}{E_{D,\rm proj}} \frac{\tau_{3,\rm tar}}{(A_{\rm tar}+A_{\rm proj}) q_{E1}} \left(\frac{NZ}{A} \right)_{\rm proj} \frac{3\hbar^2}{4m_{\rm proton}}. \quad (17)$$

By making the crude approximation $\langle \psi_i | r_{\rm tar} | \psi_f \rangle \sim \langle r_{\rm tar} \rangle$, we can estimate the ratio of the amplitudes for semidirect excitation of the projectile and the target to be ~ -1 for ^{3}He + ^{148}Sm. Thus the amplitude for exciting the GDR of the ^{3}He is of the same order as that for semidirect target excitation by the ^{3}He, and the phase is opposite. Since the centroid of the GDR (i.e., the centroid for photoabsorption) of the ^{3}He is only at $\approx$ 15 MeV [40–42], i.e., about the same energy as or lower than the targets used here, the calculated cross section for radiation from this projectile excitation is about the same as that for target excitation, and thus is very small.

The isovector potential strength $V_1(0)$ for exciting the α is not known; we take the strength to be the same as that for exciting the ^{3}He, and take the functional form to be the same as the Dabrowski optical potential for α's used above. Since the GDR centroid of the α is at 25 MeV [43–45], and the experimental cross section for the α-induced reactions is smaller, one might expect the yield to be significant. The result of our distorted-wave (DW) estimate is shown in Fig. 15; although the yield from excitation of the α appears significant compared to direct radiative capture, the coherent sum of the two processes is not much larger than the direct contribution.

Our assumptions that the α maintains its integrity throughout the semidirect process, and that it has a GDR unaffected by the mean field of the target, are rather crude; nevertheless, our estimate indicates that semidirect projectile excitation may not be completely negligible.

E. Other calculations and measurements

Nakayama and Bertsch [46] have performed potential bremsstrahlung calculations of 27 MeV α+^{154}Sm and ^{3}He+^{148}Sm. In their calculations, a He projectile plane wave is incident on a one-dimensional step potential with a Woods-Saxon shape. Their results are cross sections which vary more slowly with E_γ than do the data, and magnitudes that lie below the data except near the end point where they agree with experiment. The ^{3}He+^{148}Sm results are similar in magnitude to the direct capture calculations presented here, while the α+^{154}Sm results are somewhat larger than our direct α+^{148}Sm calculations. The potential bremsstrahlung calculations of Nakayama and Bertsch are similar in principle to the present direct capture calculations, the primary difference being the manner in which the final state is treated.

Recently, measurements and calculations of photon production cross sections for 40 and 50 MeV α–nucleus collisions have been published by Sharan *et al.* [47]. The experimental results are qualitatively similar to ours, with large nonstatistical yields for γ-ray energies above the GDR, and forward-peaked angular distributions. The nonstatistical cross-section magnitudes and slopes are larger than our results, as one would expect from the higher bombarding energies. Sharan *et al.* report both potential bremsstrahlung and nucleon-nucleon bremsstrahlung calculations following the general methods of Nakayama and Bertsch. At high E_γ the sum of the two shows a much flatter E_γ dependence than the data, and exceeds the data at the highest energies.

Measurements [5] of the spectral shape of high-energy γ rays emitted in ^{6}Li+^{98}Mo and ^{6}Li+^{181}Ta collisions show evidence for a nonstatistical enhancement at the highest γ-ray energies, $E_\gamma = 20$ to 25 MeV. The enhancement appears similar to that observed in this work for α-induced reactions at low E_α. The properties of these reactions are included in Table I.

Calculations of preequilibrium γ emission using a hybrid model have been performed by Obložinský [48,49] and by Reffo *et al.* [50]. In these calculations the projectile dissolves in the target nucleus and the total energy of the reaction is shared by the projectile nucleons, which may individually excite the GDR via a semidirect process. When the corrections of Obložinský [49] are included, the results of the two groups are similar, with a spectrum shape in rough agreement with experiment, and a magnitude lower than experiment by about a factor of 2. Given the schematic manner in which the preequilibrium semidirect GDR excitation is treated, one should probably not expect better than order-of-magnitude agreement [51]. Also, although it has been argued [51,48] that the model treats the γ-ray emission rate in a manner consistent with the equilibrium statistical model, these calculations fail in the equilibrium region by four orders of magnitude [48].

V. CONCLUSION

We have measured high-energy γ-ray yields from ^{3}He- and α-induced reactions. The observed yields cannot be explained by a statistical reaction mechanism. The front-back angular asymmetry of the yields provides model-independent evidence that the γ-ray production is nonstatistical. The slopes and magnitudes of the yields appear to depend on the total energy available in the reaction, and perhaps also on the $E1$ effective charge.

Our direct-semidirect radiative capture calculations can reproduce the strongly forward-peaked angular distributions and cross-section magnitudes at the highest γ-ray energies. However, such reactions in which the projectile maintains its integrity during the capture process are all characterized by one-body level densities for the composite particle in the final state. Because these densities vary slowly with excitation energy, the resulting calculated spectra vary slowly with γ-ray energy. Hence the bulk of the nonstatistical, exponentially falling yield for $E_\gamma > E_{\rm GDR}$ must be due to some other process.

The slopes of the high-energy γ yields suggest a final-state level density which grows with excitation energy, though not as rapidly as the full level density which enters in statistical decay. This tends to rule out simple direct and semidirect capture and favors some sort of preequilibrium mechanism. Hybrid models [48–50] that include excitons which excite the GDR are able to approximately reproduce the shape of the ^{3}He+^{148}Sm and α+^{154}Sm spectra.

Recently a major step forward has been achieved in the understanding of nucleon radiative capture with an extended direct-semidirect model which includes, for the first time, capture into virtual single-particle configurations which then damp into the compound nucleus [52]. This feature is essential for reproducing the strength of the nonstatistical GDR bump observed in γ-ray spectra from the ^{89}Y(p,γ) reaction, for $E_\gamma \sim E_{\rm GDR}$, at bombarding energies where the bump corresponds to γ-decay to unbound states. It would be very interesting to see the results of similar model calculations for ^{3}He- and α-induced reactions.

[1] K. A. Snover, Annu. Rev. Nucl. Part. Sci. **36**, 545 (1986).

[2] W. Cassing, V. Metag, U. Mosel, and K. Niita, Phys. Rep. **188**, 364 (1990).

[3] R. Heuer, B. Muller, H. Stocker, and W. Greiner, Z. Phys. A **330**, 315 (1988).

[4] F. Pühlhofer, Nucl. Phys. **A280**, 267 (1977).

[5] M. Kicińska-Habior, K. A. Snover, C. A. Gossett, J. A. Behr, G. Feldman, H. K. Glatzel, J. H. Gundlach, and E. F. Garman, Phys. Rev. C **36**, 612 (1987).

[6] G. Feldman, K. A. Snover, J. A. Behr, C. A. Gossett, J. H. Gundlach, and M. Kicinska-Habior, Phys. Rev. C **47**, 1436 (1993).

[7] M. N. Harakeh, D. H. Dowell, G. Feldman, E. F. Garman, R. Loveman, J. L. Osborne, and K. A. Snover, Phys. Lett. B **176**, 297 (1986).

[8] F. Ajzenberg-Selove, Nucl. Phys. **A433**, 1 (1985).

[9] F. Ajzenberg-Selove, Nucl. Phys. **A449**, 1 (1986).

[10] M. N. Harakeh, P. Paul, H. M. Kuan, and E. K. Warburton, Phys. Rev. C **12**, 1410 (1975).

[11] See, for example, F. S. Dietrich, D. W. Heikkinen, K. A. Snover, and K. Ebisawa, Phys. Rev. Lett. **38**, 156 (1977).

[12] N. Shikazono and T. Terasawa, Nucl. Phys. **A250**, 260 (1975).

[13] B. L. Berman and S. C. Fultz, Rev. Mod. Phys. **47**, 713 (1975).

[14] N. Herrmann, R. Bock, H. Emling, R. Freifelder, A. Gobbi, E. Grosse, K. D. Hildenbrand, R. Kulessa, T. Matulewicz, F. Rami, R. S. Simon, H. Stelzer, J. Wessels, P. R. Maurenzig, A. Olmi, A. A. Stefanini, W. Kühn, V. Metag, R. Novotny, M. Gnirs, D. Pelte, P. Braun-Munzinger, and L. G. Moretto, Phys. Rev. Lett. **60**, 1630 (1988).

[15] W. Reisdorf, Z. Phys. A **300**, 227 (1981).

[16] D. Vermeulen, H. G. Clerc, C. C. Sahm, K. H. Schmidt, J. G. Keller, G. Münzenberg, and W. Reisdorf, Z. Phys. A **318**, 157 (1984); C. C. Sahm, H. G. Clerc, K. H. Schmidt, W. Reisdorf, P. Armbruster, F. P. Hesseberger, J. G. Keller, G. Münzenberg, and D. Vermeulen, Nucl. Phys. **A441**, 316 (1985).

[17] M. Kicińska-Habior, K. A. Snover, J. A. Behr, G. Feldman, C. A. Gossett, and J. H. Gundlach, Phys. Rev. C **41**, 2075 (1990).

[18] F. Cohen, F. Plasil, and W. J. Swiatecki, Ann. Phys. (N.Y.) **82**, 557 (1974).

[19] A. DeShalit and H. Feshbach, *Theoretical Nuclear Physics Volume 1: Nuclear Structure* (John Wiley & Sons, New York, 1974), pp. 346ff.

[20] H. T. Fortune, M. N. I. Al-Jadir, R. R. Betts, J. N. Bishop, and R. Middleton, Phys. Rev. C **19**, 756 (1979).

[21] H. W. Fulbright, C. L. Bennett, R. A. Lindgren, R. G. Markham, S. C. McGuire, G. C. Morrison, U. Strohbusch, and

J. Toke, Nucl. Phys. **A284**, 329 (1977).
[22] J. Jänecke, F. D. Becchetti, D. Overway, and C. E. Thorn, Phys. Rev. C **26**, 405 (1982).
[23] A. M. Van den Berg, A. Saha, G. D. Jones, L. W. Put, and R. H. Siemssen, Nucl. Phys. **429**, 1 (1984), and references therein.
[24] J. Jänecke, F. D. Becchetti, D. Overway, J. D. Cossairt, and R. L. Spross, Phys. Rev. C **23**, 101 (1981), and references therein.
[25] F. Michel, G. Reidemeister, and S. Ohkubo, Phys. Rev. Lett. **57**, 1215 (1986).
[26] B. Buck, C. B. Dover, and J. P. Vary, Phys. Rev. C **11**, 1803 (1975).
[27] E. Hagberg, P. G. Hansen, P. Hornshoj, B. Jonson, S. Mattsson, and P. Tidemand-Petersson, Phys. Lett. **73B**, 139 (1978), and references therein.
[28] H. Dabrowski and L. Freindl, Acta Phys. Pol. **B12**, 703 (1981).
[29] A. A. Aponik, Jr., C. M. Chesterfield, D. A. Bromley, and N. K. Glendenning, Nucl. Phys. **A159**, 367 (1970).
[30] G. R. Satchler, *Direct Nuclear Reactions* (Oxford University Press, Oxford, 1983), pp. 525ff, and references therein.
[31] M. Hyakutake, I. Kumabe, M. Fukada, T. Komatuzaki, T. Yamagata, M. Inoue, and H. Ogata, Nucl. Phys. **A333**, 1 (1980).
[32] C. F. Clement, A. M. Lane, and J. R. Rook, Nucl. Phys. **66** 273, 293 (1965).
[33] M. Potokar, Phys. Lett. **46B**, 346 (1973).
[34] M. Potokar, A. Likar, M. Budnar, and F. Cvelbar, Nucl. Phys. **A277**, 29 (1977).
[35] G. R. Satchler, Nucl. Phys. **A195**, 1 (1972).
[36] K. Ebisawa, Ph.D. thesis, University of Washington, 1978: note that this thesis has typographical errors pointed out by T. Murakami (private communication).
[37] G. R. Satchler, Nucl. Phys. **A472**, 215 (1987).
[38] C. F. Clement and S. M. Perez, Phys. Lett. **33B**, 391 (1970).
[39] L. Ray, W. Rory Coker, and G. W. Hoffmann, Phys. Rev. C **18**, 2641 (1978).
[40] B. L. Berman, L. J. Koester, Jr., and J. H. Smith, Phys. Rev. **133**, B117 (1964).
[41] B. L. Berman, S. C. Fultz, and P. F. Yergin, Phys. Rev. Lett. **24**, 1494 (1970).
[42] G. Ticcioni, S. N. Gardiner, J. L. Matthews, and R. O. Owens, Phys. Lett. **46B**, 369 (1973).
[43] F. Balestra, E. Bollini, L. Busso, R. Garfagnini, C. Guarldo, G. Piragino, R. Scrimaglio, and A. Zanini, Nuovo Cimento A **38**, 145 (1977).
[44] J. D. Irish, R. G. Johnson, B. L. Berman, B. J. Thomas, K. G. Mcneill, and J. W. Jury, Can. J. Phys. **53**, 802 (1975).
[45] H. G. Clerc, R. J. Stewart, and R. C. Morrison, Phys. Lett. **18**, 316 (1965).
[46] K. Nakayama and G. F. Bertsch, Phys. Rev. C **36**, 1848 (1987).
[47] M. K. Sharan, Y. K. Agarwal, C. V. K. Baba, D. R. Chakrabarty, and V. M. Datar, Phys. Rev. C **48**, 2845 (1993).
[48] P. Obložinský, Phys. Lett. B **215**, 597 (1988).
[49] P. Obložinský, Phys. Rev. C **41**, 401 (1990).
[50] G. Reffo, M. Blann, and B. A. Remington, Phys. Rev. C **38**, 1190 (1988); **39**, 1188(E) (1989); **41**, 403 (1990).
[51] J. M. Akkermans and H. Gruppelaar, Phys. Lett. B **157**, 95 (1985).
[52] W. E. Parker, M. B. Chadwick, F. S. Dietrich, J. E. Kammeraad, S. J. Luke, K. E. Sale, R. M. Chasteler, M. A. Godwin, L. H. Kramer, G. J. Schmid, H. R. Weller, and A. K. Kerman, Phys. Rev. C **52**, 252, (1995).